A simplified calculation for adaptive coefficients of finite-difference frequency-domain method

Xu Wen-Hao[1], Ba Jing[1]*, Carcione José Maria[1,2], Yang Zhi-Fang[3,4], and Yan Xin-Fei[3,4]

Abstract: The finite-difference frequency domain (FDFD) method is widely applied for simulating seismic wavefields, and a key to achieving successful FDFD simulation is to construct FDFD coefficients that can effectively suppress numerical dispersion. Among the existing FDFD coefficients for seismic wavefield simulation, adaptive FDFD coefficients that vary with the number of wavelengths per grid can suppress numerical dispersion to the maximum extent. The current methods for calculating adaptive FDFD coefficients involve numerical integration, conjugate gradient (CG) optimization, sequential initial value selection, and smooth regularization, which are difficult to implement and inefficient in calculations. To simplify the calculation of adaptive FDFD coefficients and improve the corresponding computational efficiency, this paper proposes a new method for calculating adaptive FDFD coefficients. First, plane-wave solutions with different discrete propagation angles are substituted in the FDFD scheme, and the corresponding least-squares problem is constructed. As this problem is ill-conditioned and obtaining smooth adaptive FDFD coefficients by the conventional solving method based on normal equations is difficult, this paper proposes solving the least-squares problem by solving the corresponding overdetermined linear system of equations through QR matrix decomposition. Compared with the existing methods for calculating adaptive FDFD coefficients based on numerical integration, CG optimization, and sequential initial value selection, the proposed method allows for a simplified computational process and considerably higher computational efficiency. Numerical wavefield simulation results show that the adaptive-coefficient FDFD method based on QR matrix decomposition can achieve the same accuracy as those based on numerical integration, CG optimization, and sequential initial value selection while requiring less computation time.

Keywords: seismic wavefield simulation, finite-difference frequency-domain method, adaptive coefficients, numerical dispersion, QR decomposition

Introduction

The finite-difference frequency-domain (FDFD) method is widely employed for seismic wavefield simulation (Štekl and Pratt, 1998; Chen, 2012; Xu and Gao, 2018). Compared with the finite-difference time-domain (FDTD) method (Virieux, 1986; Zhang et al., 2018; Wang et al., 2018), the FDFD method can efficiently simulate narrowband or multishot seismic

---

data, flexibly simulate seismic attenuation effects, parallelize the simulations of different frequency components of a wavefield, and avoid temporal dispersion and temporal extrapolation instability. Seismic wavefield simulations using the FDFD method usually suffer from numerical dispersion errors; thus, the construction of FDFD coefficients that can effectively suppress numerical dispersion is necessary for FDFD seismic wavefield simulations.

The existing methods for constructing FDFD coefficients in seismic wavefield simulations can be classified into three categories. The first category of methods is based on Taylor expansion. The second-order FDFD method based on Taylor expansion is a classical method in seismic wavefield simulation (Pratt and Worthington, 1990; Pratt, 1990), which is easy to implement and corresponds to an FDFD sparse coefficient matrix with a small bandwidth. However, wavefield simulation based on the second-order FDFD method requires a large number of grid points per wavelength (Jo et al., 1996), which leads to the requirement of more discrete sampling points, thereby resulting in a large FDFD coefficient matrix that is difficult to be solved efficiently. By taking the two-dimensional (2D) acoustic wave equation as an example and the relative phase velocity error not exceeding 1% as a criterion, the number of grid points per wavelength required for the corresponding numerical simulation with the second-order FDFD method is found to be 13 (Chen, 2012). Meanwhile, similar to the coefficients based on high-order Taylor expansions commonly used in FDTD methods (Dablain, 1986; Gao et al., 2018), coefficients based on high-order Taylor expansions can also be used in FDFD methods (Xu et al., 2021a). The implementation of wavefield simulations based on the high-order FDFD method is easy and requires few grid points per wavelength. However, the high-order FDFD corresponds to a large bandwidth of the FDFD sparse coefficient matrix, which is difficult to solve for multiple shots with a direct solver. Furthermore, the coefficient matrix contains more nonzero elements, requiring great computational efforts while employing an iterative solver (Xu et al., 2021b).

The second category involves optimal FDFD coefficients. To reduce the number of grid points per wavelength required by the traditional second-order FDFD method and avoid the large matrix bandwidth of the high-order FDFD method, optimal FDFD coefficients that optimize numerical dispersion over

a range of wavenumbers are utilized (Štekl and Pratt, 1998; Min et al., 2000; Chen, 2012). Optimal FDFD coefficients are obtained using the plane-wave solution of the wave equation to derive the explicit numerical-dispersion relation, selecting an appropriate range of the number of wavelengths per grid (NWPG), and then optimizing numerical dispersion within that range to obtain the FDFD coefficients. Compared with the traditional second-order FDFD method, the optimal-coefficient FDFD method can effectively reduce the required number of grid points per wavelength. By taking the 2D acoustic wave equation as an example, the number of grid points per wavelength required for numerical simulation using the optimal nine-point FDFD method is found to be 4 (Jo et al., 1996; Chen, 2012), while that using the optimal 25-point FDFD can be reduced to 2.13 (Shin and Sohn, 1998; Zhang et al., 2014; Fan et al., 2017). Although the optimal 25-point FDFD method can well suppress numerical dispersion even when the number of grid points per wavelength is close to the Nyquist sampling limit, the sparse coefficient matrix of the FDFD corresponding to the method has a larger bandwidth and more nonzero elements compared to the second-order FDFD method and the optimal nine-point FDFD method. Consequently, a greater computational effort is required to solve the corresponding sparse linear equation system (Xu and Gao, 2018). Moreover, although the optimal FDFD method can effectively reduce the required number of grid points per wavelength compared to the traditional second-order FDFD method, the numerical dispersion error corresponding to each NWPG is not fully minimized. This is because the optimal FDFD method considers numerical errors corresponding to more than one NWPG when the same FDFD coefficients are used for different NWPGs (Aghamiry et al., 2022).

The third category involves adaptive FDFD coefficients that assume different values for different NWPGs. On the basis of the 2D acoustic wave equation, Xu and Gao (2018) proposed adaptive FDFD coefficients that vary with NWPG. For the adaptive FDFD coefficients, the plane-wave solution of the wave equation is substituted into the FDFD discrete scheme, and the corresponding adaptive FDFD coefficients are obtained by minimizing the substitution error of the plane-wave solution for different NWPGs. Further, to avoid calculating the adaptive FDFD coefficients for each discrete point of the model, which is computationally intensive, Xu and Gao (2018) proposed the calculation

of adaptive FDFD coefficients for NWPGs sampled from 0 to 0.5 with a small sampling interval before wavefield simulation, thereby constructing a lookup table for adaptive FDFD coefficients. The lookup table enables the improvement of the optimal FDFD coefficients through adaptive ones with negligible extra computational cost compared with the cost of a wavefield simulation (Xu and Gao, 2018; Aghamiry et al., 2022). Xu et al. (2021b) extended the adaptive-coefficient FDFD method to the three-dimensional (3D) acoustic wave equation and proposed a general adaptive-coefficient FDFD scheme that is easy to generalize and implement. Aghamiry et al. (2022) verified that the adaptive-coefficient FDFD method can simulate 3D large-scale complex models with high accuracy and can simulate models with sharp contrast more accurately than the presently employed temporal second-order and spatial eighth-order FDTD methods. Compared with the optimal FDFD method, the adaptive-coefficient FDFD method can reduce the numerical dispersion error corresponding to each NWPG and reduce the required number of grid points per wavelength. By taking the 2D acoustic wave equation as an example, the required number of grid points per wavelength for the numerical simulation using the adaptive-coefficient nine-point FDFD method can be reduced to 2.12 (Xu and Gao, 2018). Thus, the adaptive-coefficient nine-point FDFD method can achieve accuracy comparable to that of the optimal 25-point FDFD method. In addition, the computational cost and computer memory required are comparable to those of the optimal nine-point FDFD method. Due to the superiority of the adaptive-coefficient FDFD method over its optimal-coefficient counterpart, it has been successfully employed in 3D large-scale full-waveform inversions (Aghamiry et al., 2022; Tournier et al., 2022; Operto et al., 2023).

Among the existing FDFD coefficients for seismic wavefield simulation, adaptive FDFD coefficients have the advantage of maximizing numerical dispersion suppression. However, the current methods for calculating adaptive FDFD coefficients are difficult to implement and computationally inefficient. The method employed by Xu and Gao (2018) and Xu et al. (2021b) to calculate adaptive FDFD coefficients involves numerical integration and conjugate gradient (CG) optimization. Further, it requires using the adaptive FDFD coefficients obtained for larger NWPGs as initial values for the iterative optimization of the adaptive FDFD coefficients corresponding to smaller NWPGs to ensure the smoothness of the obtained adaptive FDFD coefficients. Although the method for calculating adaptive coefficients adopted by Aghamiry et al. (2022) avoids numerical integration and iterative optimization, a large-scale overdetermined linear system needs to be solved. Further, the overdetermined linear system contains a smooth regularization term to ensure the smoothness of the obtained adaptive coefficients. However, Aghamiry et al. (2022) did not provide a specific construction scheme for the corresponding smooth regularization term.

To simplify the calculation of the adaptive FDFD coefficients and improve the corresponding computational efficiency, a new method for calculating the coefficients is proposed herein. First, plane-wave solutions with different discrete propagation angles are substituted into the FDFD scheme, and the corresponding least-squares problem is constructed. Since this least-squares problem is ill-conditioned and obtaining smooth adaptive FDFD coefficients by conventional methods based on normal equations (NEs) is difficult, this paper proposes solving the least-squares problem by solving the corresponding overdetermined linear system of equations through QR matrix decomposition. To verify the effectiveness of the proposed method, the QR adaptive FDFD coefficients obtained by the proposed QR method are compared with the CG adaptive FDFD coefficients obtained by Xu et al. (2021b) based on numerical integration, CG optimization, and sequential initial value selection. In addition, the computational times required in both methods are compared. Meanwhile, the wavefield simulation results obtained by the proposed QR adaptive-coefficient FDFD method are compared with those obtained by the CG adaptive-coefficient FDFD method reported by Xu et al. (2021b) for three typical 3D acoustic wave models, and the wavefield simulation times required by the two methods are compared.

Theory

Least-squares problem for the adaptive FDFD coefficients

In this paper, the proposed method for calculating the adaptive FDFD coefficients is illustrated based on the 3D acoustic wave equation. First, we consider the following 3D acoustic wave equation with no source in

the frequency domain:

$$\frac{\omega^2}{v^2}P+\frac{\partial^2 P}{\partial x^2}+\frac{\partial^2 P}{\partial y^2}+\frac{\partial^2 P}{\partial z^2}=0, \qquad (1)$$

where P denotes the frequency-domain wavefield, v denotes the wave propagation velocity, and ω denotes the angular frequency.

According to Xu et al. (2021b), the adaptive-coefficient 27-point FDFD discretization of equation (1) with a general scheme can be expressed as follows:

$$\frac{\omega^2}{v_{m,n,l}^2}P_{m,n,l}+\frac{1}{\Delta x^2}\left(P_{m-1,n,l}+P_{m+1,n,l}-2P_{m,n,l}\right)$$

$$+\frac{1}{\Delta y^2}\left(P_{m,n-1,l}+P_{m,n+1,l}-2P_{m,n,l}\right)$$

$$+\frac{1}{\Delta z^2}\left(P_{m,n,l-1}+P_{m,n,l+1}-2P_{m,n,l}\right)$$

$$+C\left(n_{\text{wpg}}^x\,\middle|\,r_1,r_2\right)=0, \qquad (2a)$$

$$C\left(n_{\text{wpg}}^x\,\middle|\,r_1,r_2\right)=\left(\frac{1}{\Delta x^2}+\frac{1}{\Delta y^2}+\frac{1}{\Delta z^2}\right)$$

$$\times\left[\,\eta_1\left(n_{\text{wpg}}^x\,\middle|\,r_1,r_2\right)\left(P_{m-1,n,l}+P_{m+1,n,l}-2P_{m,n,l}\right)\right.$$

$$+\eta_2\left(n_{\text{wpg}}^x\,\middle|\,r_1,r_2\right)\left(P_{m,n-1,l}+P_{m,n+1,l}-2P_{m,n,l}\right)$$

$$+\eta_3\left(n_{\text{wpg}}^x\,\middle|\,r_1,r_2\right)\left(P_{m,n,l-1}+P_{m,n,l+1}-2P_{m,n,l}\right)$$

$$+\eta_4\left(n_{\text{wpg}}^x\,\middle|\,r_1,r_2\right)\left(P_{m-1,n-1,l}+P_{m+1,n-1,l}+P_{m-1,n+1,l}+P_{m+1,n+1,l}-4P_{m,n,l}\right)$$

$$+\eta_5\left(n_{\text{wpg}}^x\,\middle|\,r_1,r_2\right)\left(P_{m-1,n,l-1}+P_{m+1,n,l-1}+P_{m-1,n,l+1}+P_{m+1,n,l+1}-4u_{m,n,l}\right)$$

$$+\eta_6\left(n_{\text{wpg}}^x\,\middle|\,r_1,r_2\right)\left(P_{m,n-1,l-1}+P_{m,n+1,l-1}+P_{m,n-1,l+1}+P_{m,n+1,l+1}-4P_{m,n,l}\right)$$

$$+\eta_7\left(n_{\text{wpg}}^x\,\middle|\,r_1,r_2\right)\left(P_{m-1,n-1,l-1}+P_{m+1,n-1,l-1}+P_{m-1,n+1,l-1}\right.$$

$$\left.P_{m-1,n-1,l+1}+P_{m+1,n-1,l+1}+P_{m-1,n+1,l+1}+P_{m+1,n+1,l+1}-8P_{m,n,l}\right)\right], \qquad (2b)$$

where $P_{m,n,l}$ and $v_{m,n,l}$ denote the wavefield and velocity at the point $(x,\,y,\,z)=(m\Delta x,\,n\Delta y,\,l\Delta z)$, respectively, $C\left(n_{\text{wpg}}^x\,\middle|\,r_1,r_2\right)$ denotes the correction term with adaptive coefficients, $n_{\text{wpg}}^x=\Delta x/\lambda=\Delta x\omega/(2\pi v)$ denotes the NWPG along the x-direction, $r_1=\Delta x/\Delta y$ and $r_2=\Delta x/\Delta z$ denote the ratios of the 3D spatial grid sizes, and $\eta_i\left(n_{\text{wpg}}^x\,\middle|\,r_1,r_2\right)(i=1,\cdots,7)$ denotes the adaptive FDFD coefficients varying with the NWPG for the given r_1 and r_2.

To obtain the required adaptive FDFD coefficients, the following 3D plane-wave solutions along different discrete propagation angles are considered:

$$P(x,y,z)=P_0 e^{-i\frac{\omega}{v}\left[\sin\left(\theta_p\right)\cos\left(\phi_q\right)x+\sin\left(\theta_p\right)\sin\left(\phi_q\right)y+\cos\left(\theta_p\right)z\right]}, \qquad (3)$$

where P_0 denotes a constant, $i=\sqrt{-1}$ denotes an imaginary unit, θ_p $(p=1,\cdots,n_\theta)$ denotes the different angles between the z-axis and the direction of wave propagation, and ϕ_q $(q=1,\cdots,n_\phi)$ denotes the different angles between the x-axis and the projection of the wave propagation direction in the x–y plane. By substituting the plane-wave solutions with different discrete propagation angles into the adaptive-coefficient FDFD scheme in equation (2), the least-squares problem for the adaptive FDFD coefficients can be obtained by minimizing the substitution error as follows:

$$\hat{\boldsymbol{\eta}}=\arg\min_{\boldsymbol{\eta}\in R^7}\sum_{p=1}^{n_\theta}\sum_{q=1}^{n_\phi}[c_0\left(\theta_p,\phi_q\,\middle|\,n_{\text{wpg}}^x,r_1,r_2\right)$$

$$+\sum_{j=1}^{7}c_j\left(\theta_p,\phi_q\,\middle|\,n_{\text{wpg}}^x,r_1,r_2\right)\eta_j\left(n_{\text{wpg}}^x\,\middle|\,r_1,r_2\right)]^2, \qquad (4a)$$

$$c_0\left(\theta_p,\phi_q\,\middle|\,n_{\text{wpg}}^x,r_1,r_2\right)=\left[1+r_1^2+r_2^2\right]^{-1}$$

$$\times\left\{\left(2\pi n_{\text{wpg}}^x\right)^2+2\left[\cos\left(2\pi n_{\text{wpg}}^x\sin\theta_p\cos\phi_q\right)-1\right]\right.$$

$$+2r_1^2\left[\cos\left(2\pi r_1^{-1}n_{\text{wpg}}^x\sin\theta_p\sin\phi_q\right)-1\right]$$

$$\left.+2r_2^2\left[\cos\left(2\pi r_2^{-1}n_{\text{wpg}}^x\cos\theta_p\right)-1\right]\right\}, \qquad (4b)$$

$$c_1\left(\theta_p,\phi_q\,\middle|\,n_{\text{wpg}}^x,r_1,r_2\right)=2\left[\cos\left(2\pi n_{\text{wpg}}^x\sin\theta_p\cos\phi_q\right)-1\right], \qquad (4c)$$

$$c_2\left(\theta_p,\phi_q\,\middle|\,n_{\text{wpg}}^x,r_1,r_2\right)=2\left[\cos\left(2\pi r_1^{-1}n_{\text{wpg}}^x\sin\theta_p\sin\phi_q\right)-1\right], \qquad (4d)$$

$$c_3\left(\theta_p,\phi_q\,\middle|\,n_{\text{wpg}}^x,r_1,r_2\right)=2\left[\cos\left(2\pi r_2^{-1}n_{\text{wpg}}^x\cos\theta_p\right)-1\right], \qquad (4e)$$

$$c_4\left(\theta_p,\phi_q\,\middle|\,n_{\text{wpg}}^x,r_1,r_2\right)=$$

$$4\left[\cos\left(2\pi n_{\text{wpg}}^x\sin\theta_p\cos\phi_q\right)\cos\left(2\pi r_1^{-1}n_{\text{wpg}}^x\sin\theta_p\sin\phi_q\right)-1\right], \qquad (4f)$$

$$c_5\left(\theta_p,\phi_q\,\middle|\,n_{\text{wpg}}^x,r_1,r_2\right)=$$

$$4\left[\cos\left(2\pi n_{\text{wpg}}^x\sin\theta_p\cos\phi_q\right)\cos\left(2\pi r_2^{-1}n_{\text{wpg}}^x\cos\theta_p\right)-1\right], \qquad (4g)$$

$$c_6\left(\theta_p,\phi_q\,\middle|\,n_{\text{wpg}}^x,r_1,r_2\right)$$

$$=4\left[\cos\left(2\pi r_1^{-1}n_{\text{wpg}}^x\sin\theta_p\sin\phi_q\right)\cos\left(2\pi r_2^{-1}n_{\text{wpg}}^x\cos\theta_p\right)-1\right], \qquad (4h)$$

$$c_7\left(\theta_p,\phi_q\,\middle|\,n_{\mathrm{wpg}}^x,r_1,r_2\right)=8\Big[\cos\left(2\pi n_{\mathrm{wpg}}^x\sin\theta_p\cos\phi_q\right)$$
$$\times\cos\left(2\pi r_1^{-1}n_{\mathrm{wpg}}^x\sin\theta_p\sin\phi_q\right)\cos\left(2\pi r_2^{-1}n_{\mathrm{wpg}}^x\cos\theta_p\right)-1\Big],\tag{4i}$$

where $\hat{\boldsymbol{\eta}}$ denotes the optimal solution to the least-squares problem. By arranging $\{\theta_p,\phi_q\}$ in the order of first ϕ_q and then θ_p, the discrete least-squares problem in equation (4) can be converted into a matrix–vector product form as follows:

$$\hat{\boldsymbol{\eta}}=\arg\min_{\boldsymbol{\eta}\in R^7}\left\|\mathbf{A}\left(n_{\mathrm{wpg}}^x\right)\boldsymbol{\eta}-\mathbf{b}\left(n_{\mathrm{wpg}}^x\right)\right\|_2^2,\tag{5}$$

where $\mathbf{A}\left(n_{\mathrm{wpg}}^x\right)$ is a coefficient matrix with $n_\theta\times n_\phi$ rows and seven columns varying with n_{wpg}^x, $\mathbf{b}\left(n_{\mathrm{wpg}}^x\right)$ is a column vector of length $n_\theta\times n_\phi$ varying with n_{wpg}^x, and $\left\|\bullet\right\|_2$ denotes the L_2 norm of the vector.

Adaptive FDFD coefficients based on QR matrix decomposition

For the discrete least-squares problem in equation (5), a common solution method is to construct the following NE:

$$\mathbf{A}^T\left(n_{\mathrm{wpg}}^x\right)\mathbf{A}\left(n_{\mathrm{wpg}}^x\right)\boldsymbol{\eta}=\mathbf{A}^T\left(n_{\mathrm{wpg}}^x\right)\mathbf{b}\left(n_{\mathrm{wpg}}^x\right),\tag{6}$$

where T denotes the matrix transpose. However, because the condition number of $\mathbf{A}^T\left(n_{\mathrm{wpg}}^x\right)\mathbf{A}\left(n_{\mathrm{wpg}}^x\right)$ is the square of the condition number of $\mathbf{A}\left(n_{\mathrm{wpg}}^x\right)$ (Golub and Van Loan, 2013), the coefficient matrix $\mathbf{A}^T\left(n_{\mathrm{wpg}}^x\right)\mathbf{A}\left(n_{\mathrm{wpg}}^x\right)$ in equation (6) can be more ill-conditioned, which may cause the derived adaptive FDFD coefficients $\boldsymbol{\eta}$ to be unsmooth with respect to n_{wpg}^x (Aghamiry et al., 2022). To solve this problem, Aghamiry et al. (2022) added a smooth regularization term about n_{wpg}^x by jointly solving the adaptive FDFD coefficients with different n_{wpg}^x; however, the method requires solving a large system of overdeterministic linear equations, and Aghamiry et al. (2022) did not provide a specific approach to construct the corresponding smooth regularization term.

To simplify the calculation of the adaptive FDFD coefficients and improve the corresponding computational efficiency, this paper proposes a new method for calculating adaptive FDFD coefficients. Specifically, according to the theory of QR decomposition of matrices (Golub and Van Loan, 2013), the matrix $\mathbf{A}\left(n_{\mathrm{wpg}}^x\right)$ can be decomposed as follows:

$$\mathbf{A}\left(n_{\mathrm{wpg}}^x\right)=\mathbf{Q}\left(n_{\mathrm{wpg}}^x\right)\begin{bmatrix}\mathbf{R}_1\left(n_{\mathrm{wpg}}^x\right)\\\mathbf{0}\end{bmatrix},\tag{7}$$

where $\mathbf{Q}\left(n_{\mathrm{wpg}}^x\right)$ is an orthogonal matrix with $n_\theta\times n_\phi$ rows and $n_\theta\times n_\phi$ columns varying with n_{wpg}^x (i.e., $\mathbf{Q}^{-1}\left(n_{\mathrm{wpg}}^x\right)=\mathbf{Q}^T\left(n_{\mathrm{wpg}}^x\right)$), and $\mathbf{R}_1\left(n_{\mathrm{wpg}}^x\right)$ is an upper triangular matrix with seven rows and seven columns varying with n_{wpg}^x. Because multiplying a vector by an orthogonal matrix does not change the L_2 norm of the vector, the least-squares problem in equation (5) can be converted into the following form by multiplying $\mathbf{Q}^T\left(n_{\mathrm{wpg}}^x\right)$ from the left within the L_2 norm:

$$\hat{\boldsymbol{\eta}}=\arg\min_{\boldsymbol{\eta}\in R^7}\left\|\begin{bmatrix}\mathbf{R}_1\left(n_{\mathrm{wpg}}^x\right)\\\mathbf{0}\end{bmatrix}\boldsymbol{\eta}-\mathbf{Q}^T\left(n_{\mathrm{wpg}}^x\right)\mathbf{b}\left(n_{\mathrm{wpg}}^x\right)\right\|_2^2.\tag{8}$$

Let the first seven columns of $\mathbf{Q}\left(n_{\mathrm{wpg}}^x\right)$ form a submatrix $\mathbf{Q}_1\left(n_{\mathrm{wpg}}^x\right)$, and then, the optimization problem in equation (8) can be simplified as

$$\hat{\boldsymbol{\eta}}=\arg\min_{\boldsymbol{\eta}\in R^7}\left\|\mathbf{R}_1\left(n_{\mathrm{wpg}}^x\right)\boldsymbol{\eta}-\mathbf{Q}_1^T\left(n_{\mathrm{wpg}}^x\right)\mathbf{b}\left(n_{\mathrm{wpg}}^x\right)\right\|_2^2.\tag{9}$$

Because $c_j\left(\theta,\phi\,\middle|\,n_{\mathrm{wpg}}^x,r_1,r_2\right)(j=1,\cdots,7)$ forms a linearly independent set of functions, $\mathbf{A}\left(n_{\mathrm{wpg}}^x\right)$ is full column rank when $\{\theta_p,\phi_q\}$ is sampled sufficiently. Then, $\mathbf{R}_1\left(n_{\mathrm{wpg}}^x\right)$ is a full-rank upper triangular matrix, so the optimization problem in equation (9) is equivalent to solving the following system of linear equations of order 7:

$$\mathbf{R}_1\left(n_{\mathrm{wpg}}^x\right)\boldsymbol{\eta}=\mathbf{Q}_1^T\left(n_{\mathrm{wpg}}^x\right)\mathbf{b}\left(n_{\mathrm{wpg}}^x\right).\tag{10}$$

Because $\mathbf{R}_1\left(n_{\mathrm{wpg}}^x\right)$ is an upper triangular matrix, equation (10) can be solved quickly by the back substitution method (Golub and Van Loan, 2013).

When solving the adaptive FDFD coefficients with the proposed method, the part that is mainly difficult and requires computational effort is the QR decomposition of the coefficient matrix $\mathbf{A}\left(n_{\mathrm{wpg}}^x\right)$ in equation (7). However, QR decomposition has been built in most current matrix libraries, such as MATLAB, the Eigen library of C++ (Rupp et al., 2016), and the NumPy library of Python (Harris et al., 2020), so the implementation of QR decomposition is actually easy.

According to Golub and Van Loan (2013), the number

of floating-point operations required for using QR decomposition to solve the least-squares problem for a matrix with M rows and N columns ($M \geq N$) is less than $2N^2M+3N^2M$. Therefore, for the matrix $\mathbf{A}\left(n_{\mathrm{wpg}}^x\right)$ with $n_\theta n_\phi$ rows and seven columns, the number of floating-point operations required for using QR decomposition to solve the corresponding least-squares problem and obtaining the adaptive FDFD coefficients is less than $119 n_\theta n_\phi$. In contrast, for each iteration, the CG method adopted by Xu et al. (2021b) must calculate the double integral with respect to angle twice with the vector dot product in the integral term, so the required number of floating-point operations for obtaining the corresponding adaptive FDFD coefficients is greater than $44 n_{iter} n_\theta n_\phi$, where n_{iter} represents the number of iterations of the CG method. Because the number of 3D adaptive FDFD coefficients is 7, n_{iter} is usually greater than 7. Therefore, the number of floating-point operations required by the QR method is obviously smaller than that of the CG method. In addition, it is difficult for the existing methods to calculate the adaptive FDFD coefficients in parallel with respect to different n_{wpg}^x. For example, the method by Xu et al. (2021b) must use the adaptive FDFD coefficients obtained at the larger n_{wpg}^x as the initial values for the iterative solution of the adaptive FDFD coefficients at the smaller n_{wpg}^x, whereas the method by Aghamiry et al. (2022) must jointly calculate the adaptive FDFD coefficients at different n_{wpg}^x to

impose a smooth regularization term on the adaptive FDFD coefficients. In contrast, the method proposed in this paper can calculate the adaptive FDFD coefficients at different n_{wpg}^x independently, and thus, the adaptive coefficients can be calculated in parallel with respect to n_{wpg}^x.

Meanwhile, because the orthogonal matrix $\mathbf{Q}\left(n_{\mathrm{wpg}}^x\right)$ in the adopted QR decomposition can be represented by some Householder vectors, the memory requirement for obtaining the adaptive FDFD coefficients using the QR decomposition of the matrix $\mathbf{A}\left(n_{\mathrm{wpg}}^x\right)$ with $n_\theta n_\phi$ rows and seven columns is less than the memory of $9 n_\theta n_\phi$ double-precision real numbers (Golub and Van Loan, 2013). Therefore, the memory requirement for obtaining the adaptive FDFD coefficients using the QR decomposition is negligible compared to that for solving a 3D FDFD linear system.

Figure 1 provides the adaptive FDFD coefficients obtained by the CG method of Xu et al. (2021b), the NE method based on normal equation (6), and the QR method based on QR decomposition for the case where $r_1 = r_2 = 3$, when both $\{\theta_p\}$ and $\{\phi_q\}$ are sampled within $[0, \pi/2]$ with a sampling interval of $\pi/180$. The figure shows that the NE method cannot obtain smooth adaptive FDFD coefficients in this case, whereas the QR method proposed in this paper can obtain adaptive FDFD coefficients as smooth as those of the CG method without imposing smoothness constraints.
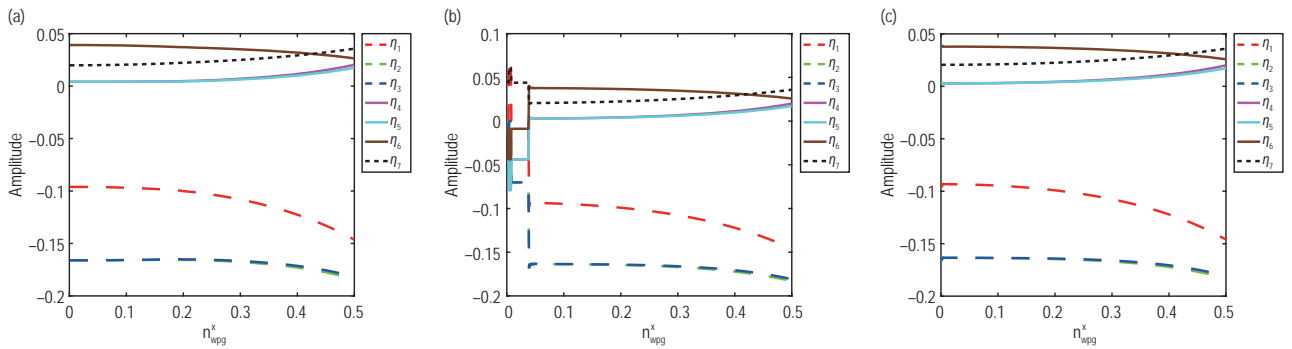
Figure 1. Comparison of the adaptive finite-difference frequency domain coefficients calculated by different methods when r_1 = 3 and r_2 = 3. (a) Conjugate gradient (CG) method based on numerical integration, CG optimization, and sequential initial value selection, and (b) normal equation (NE) method based on NEs, and (c) QR method based on QR decomposition.

Adaptive FDFD coefficient lookup table

By the proposed QR method, we can quickly and parallelly calculate adaptive FDFD coefficients for different n_{wpg}^x; however, for large 3D models, the method requires much additional computational time to calculate the coefficients at every grid point. Similar to the existing

methods for calculating adaptive FDFD coefficients (Xu and Gao, 2018; Xu et al., 2021b; Aghamiry et al., 2022), the QR method can be combined with a lookup-table technique to reduce the computational time. Particularly, after r_1 and r_2 are determined for the given model, n_{wpg}^x is sampled between 0.001 and 0.05 with a sampling

interval of 0.001, and a lookup table is generated by parallelly calculating the adaptive FDFD coefficients corresponding to the sampled n_{wpg}^x. Parts of the lookup tables of the adaptive FDFD coefficients obtained by the CG and QR methods for $r_1 = r_2 = 3$ are presented in Tables 1 and 2, respectively. The tables show that the adaptive FDFD coefficients obtained by the QR and CG methods are consistent with each other. For n_{wpg}^x absent in the lookup table, the corresponding adaptive FDFD coefficients can be obtained by the linear interpolation of

the lookup table (Xu et al., 2021b). As shown in Figure 1, the adaptive FDFD coefficients obtained by the QR method are quite smooth, and hence, linear interpolation with an interval of 0.001 can achieve high accuracy. Evidently, from the subsequent numerical examples, the numerical wavefield obtained by the QR method is in good agreement with the analytic and reference solutions, which verifies the effectiveness of linear interpolation.

Table 1 Part of the lookup table of adaptive finite-difference frequency domain coefficients for the three-dimensional acoustic wave equations obtained by the conjugate gradient method ($r_1 = r_2 = 3$)

n_{wpg}^x	η_1	η_2	η_3	η_4	η_5	η_6	η_7
0.05	−0.09625	−0.16604	−0.16601	0.00418	0.00416	0.03906	0.02000
0.10	−0.09689	−0.16589	−0.16578	0.00424	0.00418	0.03867	0.02045
0.15	−0.09804	−0.16564	−0.16539	0.00438	0.00424	0.03799	0.02122
0.20	−0.10011	−0.16568	−0.16524	0.00478	0.00453	0.03714	0.02224
0.25	−0.10332	−0.16623	−0.16555	0.00557	0.00514	0.03617	0.02352
0.30	−0.10811	−0.16765	−0.16669	0.00695	0.00628	0.03511	0.02504
0.35	−0.11442	−0.16981	−0.16855	0.00889	0.00789	0.03374	0.02693
0.40	−0.12257	−0.17297	−0.17138	0.01156	0.01011	0.03193	0.02928
0.45	−0.13304	−0.17753	−0.17562	0.01524	0.01319	0.02956	0.03217
0.50	−0.14644	−0.18411	−0.18186	0.02034	0.01746	0.02645	0.03568

Table 2 Part of the lookup table of adaptive finite-difference frequency domain coefficients for the three-dimensional acoustic wave equations obtained by the QR method ($r_1 = r_2 = 3$)

n_{wpg}^x	η_1	η_2	η_3	η_4	η_5	η_6	η_7
0.05	−0.09362	−0.16351	−0.16348	0.00286	0.00285	0.03779	0.02066
0.10	−0.09467	−0.16370	−0.16359	0.00312	0.00307	0.03757	0.02101
0.15	−0.09647	−0.16406	−0.16381	0.00358	0.00345	0.03719	0.02162
0.20	−0.09912	−0.16465	−0.16421	0.00428	0.00403	0.03662	0.02249
0.25	−0.10277	−0.16558	−0.16491	0.00528	0.00486	0.03582	0.02367
0.30	−0.10762	−0.16698	−0.16604	0.00667	0.00602	0.03475	0.02519
0.35	−0.11394	−0.16908	−0.16784	0.00860	0.00762	0.03333	0.02709
0.40	−0.12210	−0.17217	−0.17060	0.01126	0.00984	0.03145	0.02946
0.45	−0.13260	−0.17666	−0.17476	0.01493	0.01291	0.02900	0.03236
0.50	−0.14606	−0.18316	−0.18091	0.02002	0.01720	0.02579	0.03590

To verify that the proposed QR method can calculate the adaptive FDFD coefficients more efficiently than the CG method adopted by Xu et al. (2021b), Table 3 provides a comparison of the computational times required to generate the adaptive FDFD coefficient lookup tables using the CG and QR methods for different r_1 and r_2, where the computational platform is a supercomputer CPU node (56 cores, 192 GB of memory, CPU type as Intel® Xeon® Gold 6258R Processor @2.7 GHz). Table 3 shows that compared

to the CG method used by Xu et al. (2021b), the QR method proposed in this paper can substantially reduce the computational time required to calculate the adaptive FDFD coefficients, especially when r_1 and r_2 are large.

Absorbing boundary with the adaptive FDFD coefficients

The adaptive FDFD coefficients in equation (2) are applied to the 3D acoustic wave equations with no source

and no boundary conditions, while practical wavefield simulations often require absorption boundaries to suppress boundary reflections. On the basis of Xu et al. (2021b), where the adaptive FDFD coefficients were applied to the perfectly matched layer (PML) (Liu and Tao, 1997; Ren and Liu, 2013) absorbing boundary, this paper further applies the adaptive FDFD coefficients to the complex-frequency-shifted PML (CFS-PML) that can better absorb the grazing incidence waves (Komatitsch and Martin, 2007; Xu et al., 2023) compared with the PML. For this purpose, the 3D acoustic wave equation with the source term and the CFS-PML absorbing boundary is given as follows:

Table 3 Comparison of the computational times (in seconds) required to generate the adaptive finite-difference frequency domain coefficient lookup tables by the conjugate gradient and QR methods for different r_1 and r_2

r_2	r_2	CG method	QR method
1	1	11	0.21
1	2	13	0.17
2	2	50	0.26
2	3	70	0.19
3	3	82	0.17
3	4	74	0.22
4	4	106	0.18
4	5	106	0.22
5	5	130	0.17

$$\frac{\omega^2}{v^2}P + \left[\begin{array}{l} \frac{1}{\xi_x}\frac{\partial}{\partial x}\left(\frac{1}{\xi_x}\frac{\partial P}{\partial x}\right) + \frac{1}{\xi_y}\frac{\partial}{\partial y}\left(\frac{1}{\xi_y}\frac{\partial P}{\partial y}\right) \\ + \frac{1}{\xi_z}\frac{\partial}{\partial z}\left(\frac{1}{\xi_z}\frac{\partial P}{\partial z}\right) \end{array} \right]$$
$$= -f(\omega)\delta(x-x_s)\delta(y-y_s)\delta(z-z_s), \quad (11)$$

where $f(\omega)$ denotes the source function, (x_s, y_s, z_s) denotes the source location, $\delta(x)$ denotes the Dirac function, $\xi_\tau = 1 + \dfrac{\xi_0^\tau(\tilde{\tau}/L_\tau)^2}{\alpha_{\max}(1-\tilde{\tau}/L_\tau)+i\omega}$, $\tau \in \{x,y,z\}$, $\xi_0^\tau = \ln(1/R)3v_{\max}/(2L_\tau)$, R denotes the theoretical boundary reflection coefficient (taken as 10^{-3} in this paper), $v_{\max}$ denotes the maximum propagation velocity, L_τ denotes the thickness of the CFS-PML in the τ-direction, $\tilde{\tau}$ denotes the distance from the inner computational region along the τ-direction, $v_{\max} = \pi f_0$, and f_0 denotes the dominant frequency of the source. After discretizing equation (11) with virtual half-grid

points and second-order finite differences and adding the correction term with the adaptive FDFD coefficients in equation (2) (Xu et al., 2021b), the adaptive-coefficient 27-point FDFD of the 3D acoustic wave equation with the CFS-PML absorbing boundary and the source term is obtained as

$$\frac{\omega^2}{v_{m,n,l}^2}P_{m,n,l}$$
$$+\frac{1}{\Delta x^2}\frac{1}{\xi_{x_m}}\left[\begin{array}{l} \frac{1}{\xi_{x_{m-0.5}}}P_{m-1,n,l} + \frac{1}{\xi_{x_{m+0.5}}}P_{m+1,n,l} \\ -\left(\frac{1}{\xi_{x_{m-0.5}}}+\frac{1}{\xi_{x_{m+0.5}}}\right)P_{m,n,l} \end{array} \right]$$
$$+\frac{1}{\Delta y^2}\frac{1}{\xi_{y_n}}\left[\begin{array}{l} \frac{1}{\xi_{y_{n-0.5}}}P_{m,n-1,l} + \frac{1}{\xi_{y_{n+0.5}}}P_{m,n+1,l} \\ -\left(\frac{1}{\xi_{y_{n-0.5}}}+\frac{1}{\xi_{y_{n+0.5}}}\right)P_{m,n,l} \end{array} \right]$$
$$+\frac{1}{\Delta z^2}\frac{1}{\xi_{z_l}}\left[\begin{array}{l} \frac{1}{\xi_{z_{l-0.5}}}P_{m,n,l-1} + \frac{1}{\xi_{z_{l+0.5}}}P_{m,n,l+1} \\ -\left(\frac{1}{\xi_{z_{l-0.5}}}+\frac{1}{\xi_{z_{l+0.5}}}\right)P_{m,n,l} \end{array} \right]$$
$$+C\left(n_{\mathrm{wpg}}^x\big|r_1,r_2\right) = -\frac{f(\omega)\delta_{m,m_s}\delta_{n,n_s}\delta_{l,l_s}}{\Delta x\Delta y\Delta z}, \quad (12)$$

where $C\left(n_{\mathrm{wpg}}^x\big|r_1,r_2\right)$ denotes the correction term with the adaptive FDFD coefficients in equation (2b), $\delta_{m,n}$ denotes the Kronecker function, and (m_s,n_s,l_s) denotes the index of the source grid point.

Numerical examples

To verify the effectiveness of the adaptive FDFD coefficients calculated by the proposed QR method, three typical 3D acoustic wave models are considered herein, and the wavefield simulation results obtained by the QR adaptive-coefficient FDFD method are compared with those obtained by the optimal 27-point FDFD method based on average-derivative method (ADM) (Chen, 2014) and the CG adaptive-coefficient FDFD method (Xu et al., 2021b). For all the following examples, 30 supercomputer CPU nodes (56 cores, 192 GB memory, CPU type: Intel® Xeon® Gold 6258R Processor @2.7 GHz) were used as the computational platform. The simulations of the wavefield components at different

frequencies were performed in parallel on different nodes through the message-passing interface.

Wavefield simulation of a 3D homogeneous model

We considered a homogeneous model with the number of grid points being 61×61×61; a model velocity of 2000 m/s; CFS-PML absorbing boundary layers of 10, 20, and 30 along the x-, y-, and z-directions, respectively; and grid sizes of $\Delta x = 33$ m, $\Delta y = 16.5$ m, and $\Delta z = 11$ m. The source was a Ricker wavelet with a dominant frequency of 10 Hz and placed at the center of the model. Further, the maximum simulated frequency was 30 Hz, and the frequency sampling interval was 1 Hz. The frequency-domain seismogram was converted into a time domain wherein the maximum time of conversion was 1 s and the time sampling interval was 1 ms. The receivers were placed from $(x, y, z) = (0$ m, 495 m, 0 m) to $(x, y, z) = (990$ m, 495 m, 0 m) along the

x-direction. The CG adaptive FDFD coefficients (Xu et al., 2021b), NE adaptive FDFD coefficients based on NEs, and QR adaptive FDFD coefficients based on QR decomposition used in this model are shown in Figure 2. Figure 3 shows the time-domain seismograms obtained by the ADM optimal 27-point FDFD, CG adaptive-coefficient 27-point FDFD, NE adaptive-coefficient 27-point FDFD, and QR adaptive-coefficient 27-point FDFD methods. Figure 4 shows the analytic solution (Chen, 2012) and single-trace time-domain seismograms at $(x, y, z) = (0$ m, 495 m, 0 m) obtained by the four aforementioned FDFD methods. Figure 2 shows that for this homogeneous model, the proposed QR method can obtain smooth adaptive FDFD coefficients comparable to those obtained by the CG method without imposing smoothness constraints; however, smooth adaptive FDFD coefficients are not obtained by the NE method. Figures 3 and 4 show that the accuracies of the wavefield simulation by the QR and CG adaptive-coefficient
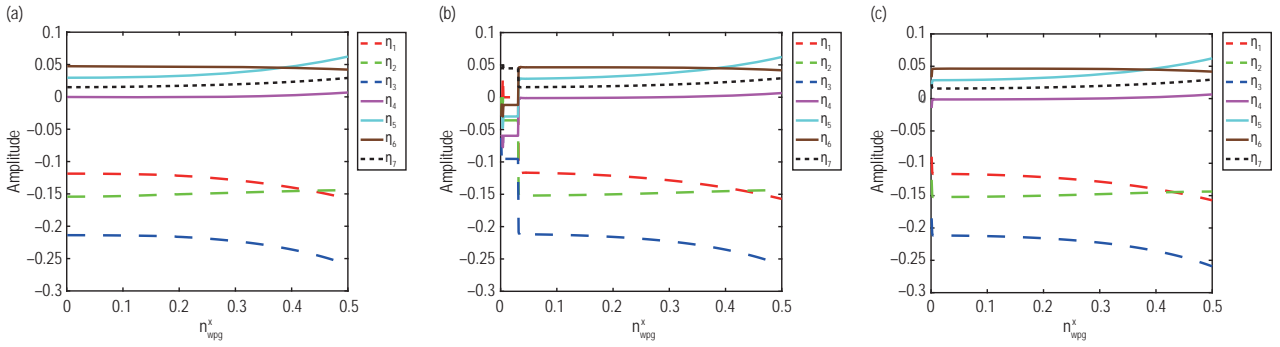
Figure 2. Adaptive finite-difference frequency domain (FDFD) coefficients corresponding to the three-dimensional homogeneous model ($r_1 = 2$, $r_2 = 3$). (a) Conjugate gradient adaptive FDFD coefficients (Xu et al., 2021b), (b) normal equation adaptive FDFD coefficients, and (c) QR adaptive FDFD coefficients.
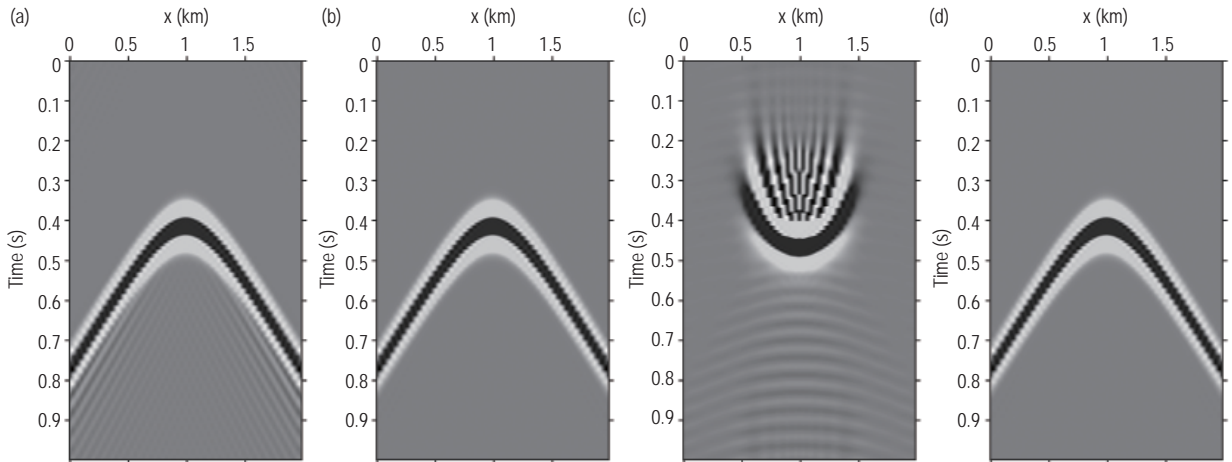
Figure 3. Seismograms obtained by different methods for the three-dimensional homogeneous model. (a) ADM optimal 27-point finite-difference frequency domain (FDFD) method, (b) conjugate gradient adaptive-coefficient 27-point FDFD method, (c) normal equation adaptive-coefficient 27-point FDFD method, and (d) QR adaptive-coefficient 27-point FDFD method.

FDFD methods are identical, and both can effectively reduce the wavefield simulation error of the ADM optimal 27-point FDFD method; however, reasonable wavefield simulation results are not obtained by the NE adaptive-coefficient FDFD method. Further, the total computational durations of the CG and QR adaptive-coefficient FDFD methods on 30 supercomputer nodes were 146 and 86 s, respectively, when the PARDISO direct solver (Petra et al., 2014a, 2014b) was used for solving the sparse linear equation system of FDFD. Therefore, for this homogeneous model, the QR adaptive-coefficient FDFD method proposed herein can considerably reduce the computational time compared with the CG counterpart.
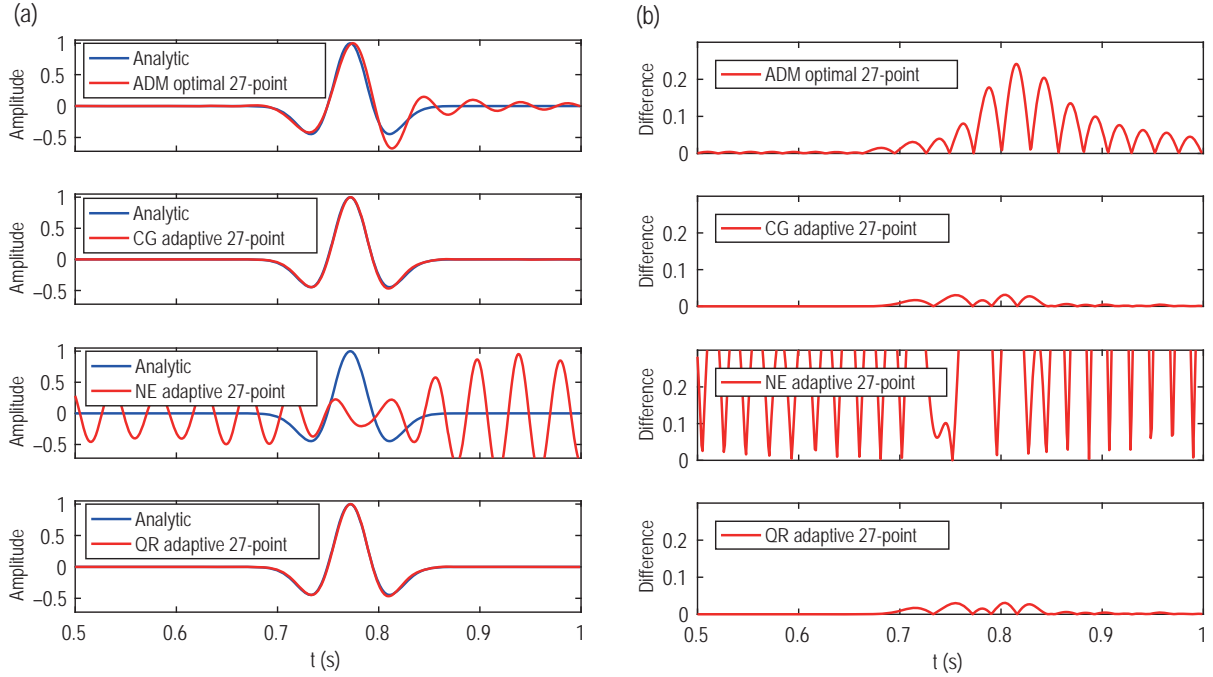
Figure 4. Analytic solution and single-trace seismograms obtained by ADM optimal 27-point finite-difference frequency domain (FDFD), conjugate gradient adaptive-coefficient 27-point FDFD, normal equation adaptive-coefficient 27-point FDFD, and QR adaptive-coefficient 27-point FDFD methods for the three-dimensional homogeneous model. Comparison of (a) amplitudes and (b) amplitude differences.

Wavefield simulation of a 3D layered model

We considered a 3D two-layer model with grid points of $61 \times 61 \times 121$, an identical thickness for the two velocity layers, constant velocities of 2000 and 4000 m/s for the first and second layers, respectively, and 10, 10, and 20 CFS-PML absorbing-boundary layers along the x-, y-, and z-directions, respectively. The grid sizes were $\Delta x = 33$ m, $\Delta y = 33$ m, and $\Delta z = 16.5$ m. Further, the source was a Ricker wavelet with a dominant frequency of 10 Hz and was placed at $(x, y, z) = (990$ m, 990 m, 165 m), the maximum simulated frequency was 30 Hz, and the frequency sampling interval was 0.5 Hz. The maximum time required to convert the frequency-domain seismogram into the time domain was 2 s, and the time sampling interval was 1 ms. The receivers were placed along the horizontal line of the x-direction at

$y = 990$ m and $z = 0$ m. This model used a high-order FDFD (72nd order in the x- and y-directions and 12th order in the z-direction) as the reference solution for the wavefield simulation (Xu et al., 2021a), and the number of orders was selected by referring to the error analysis of finite differences of different orders for different NWPGs reported by Zhang and Yao (2013). Figure 5 shows the CG adaptive FDFD coefficients (Xu et al., 2021b) and QR adaptive FDFD coefficients corresponding to this model. Figure 6 shows wavefield snapshots at 0.75 s obtained by the ADM optimal 27-point FDFD, CG adaptive-coefficient 27-point FDFD, and QR adaptive-coefficient 27-point FDFD methods and the reference solution. Figure 7 shows the seismograms obtained by the four aforementioned methods. Figure 8 shows the single-trace time-domain seismograms obtained at $(x,$

y, z) = (0 m, 990 m, 0 m) by the reference solution and the other three FDFD methods. Figures 6–8 show that for the 3D layered model, the wavefield simulation accuracies of the QR and CG adaptive-coefficient FDFD

methods are identical, and both can effectively reduce the wavefield simulation error compared with the ADM optimal 27-point FDFD method. The total computational times of the CG and QR adaptive-coefficient FDFD
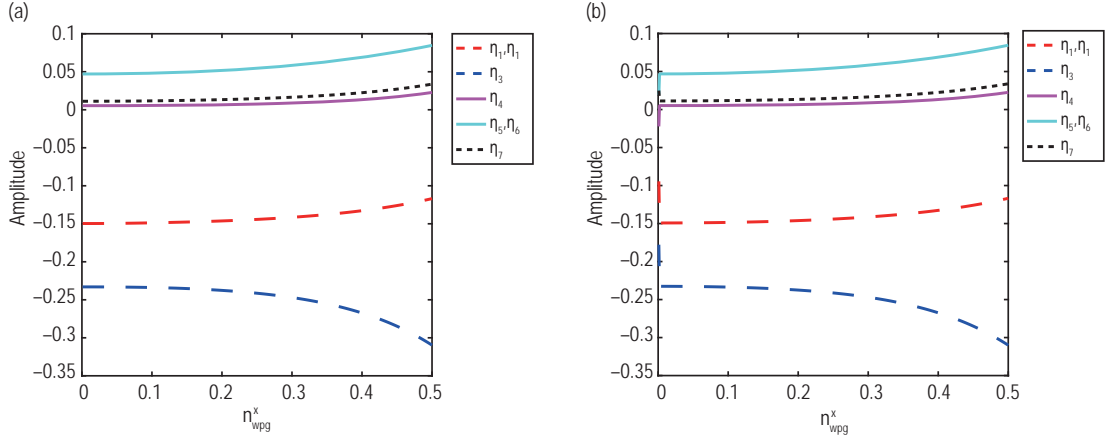
Figure 5. (a) Conjugate gradient adaptive finite-difference frequency domain (FDFD) coefficients (Xu et al., 2021b) and (b) QR adaptive FDFD coefficients corresponding to the three-dimensional layered model ($r_1 = 1$ and $r_2 = 2$).
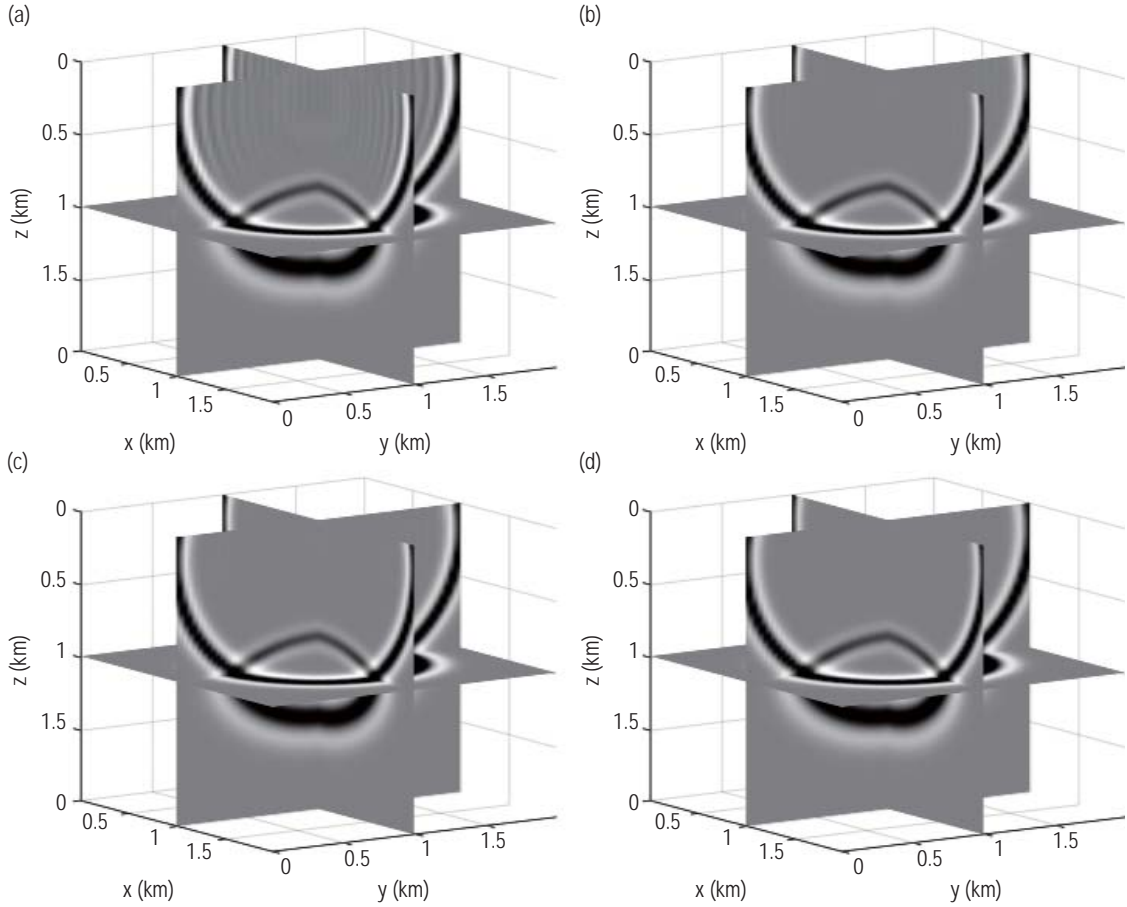
Figure 6. Wavefield snapshots obtained by different methods for the three-dimensional layered model at 0.75 s. (a) ADM optimal 27-point finite-difference frequency domain (FDFD) method, (b) conjugate gradient adaptive-coefficient 27-point FDFD method, (c) QR adaptive-coefficient 27-point FDFD method, and (d) reference solution (high-order FDFD with 72nd order in the x- and y-directions and 12th order in the z-direction).

11

methods on 30 supercomputer nodes were found to be 211 and 200 s, respectively, when the PARDISO direct solver was used for solving the FDFD sparse linear equations. Therefore, for the layered model, the proposed QR adaptive-coefficient FDFD method can reduce the required computational time of the existing CG counterpart.
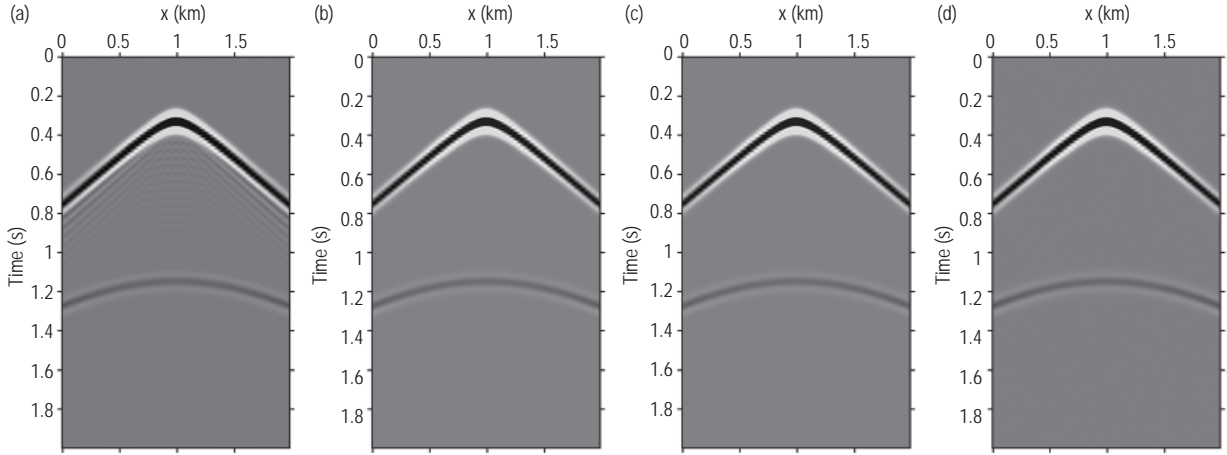
Figure 7. Seismograms obtained by different methods for the three-dimensional layered model. (a) ADM optimal 27-point finite-difference frequency domain (FDFD) method, (b) conjugate gradient adaptive-coefficient 27-point FDFD method, (c) QR adaptive-coefficient 27-point FDFD method, and (d) reference solution (high-order FDFD with 72nd order in the x- and y-directions and 12th order in the z-direction).
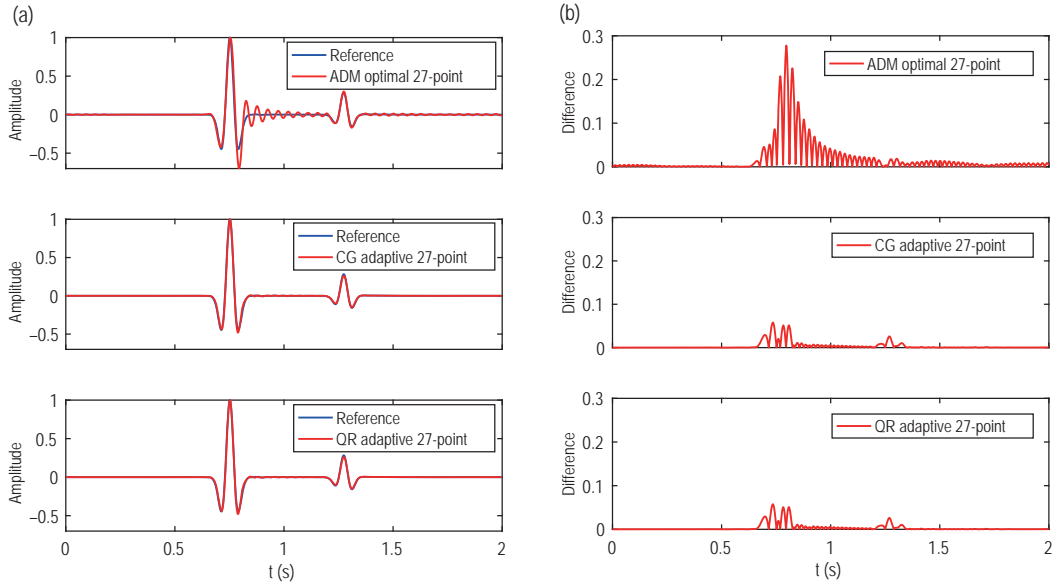
Figure 8. Comparison of the single-trace seismograms obtained by ADM optimal 27-point finite-difference frequency domain (FDFD), conjugate gradient adaptive-coefficient 27-point FDFD, and QR adaptive-coefficient 27-point FDFD with the reference solution (high-order FDFD with 72nd order in the x- and y-directions and 12th order in the z-direction) for the three-dimensional layered model. Comparison of (a) amplitudes and (b) amplitude differences.

Wavefield simulation of a 3D SEG/EAGE salt-dome model

A 3D SEG/EAGE salt-dome model with a number of grid points of 226×226×67 was considered. The number of CFS-PML absorbing boundary layers along each side of the x-, y-, and z-directions was 10, and the grid sizes were $\Delta x = \Delta y = \Delta z = 60$ m. A 3D slice of this model is given in Figure 9. The source was a Ricker wavelet with a dominant frequency of 4 Hz and was placed at (x, y, z) = (6720 m, 6720 m, 600 m). The maximum frequency simulated was 12 Hz with a frequency sampling interval

of 0.1 Hz, and the maximum time of conversion of the frequency-domain seismogram into the time domain was 10 s with a time sampling interval of 5 ms. The receivers were placed along the horizontal line of the *x*-direction at $y = 6720$ m and $z = 600$ m. This model used a high-order FDFD (72nd order in the *x*-, *y*-, and *z*-directions) as the reference solution for the wavefield simulation (Xu et al., 2021a). The CG adaptive FDFD coefficients (Xu et al., 2021b) and QR adaptive FDFD coefficients corresponding to the model are given in Figure 10. The

frequency-domain slices at 10 Hz obtained by the ADM optimal 27-point FDFD, the CG adaptive-coefficient 27-point FDFD, the QR adaptive-coefficient 27-point FDFD, and the reference solution are given in Figure 11. Figure 12 provides the vertical single-trace comparison of the frequency-domain slices in Figure 11 at $x = 13500$ m and $y = 13500$ m. Figure 13 provides a comparison of the received time-domain seismograms for the four methods. Figures 11–13 show that for the 3D salt-dome model, the wavefield simulation accuracies of the QR adaptive-coefficient FDFD and CG adaptive-coefficient FDFD are the same, and both can effectively reduce the wavefield simulation error of the ADM optimal 27-point FDFD. In addition, the total computational times of the CG adaptive-coefficient FDFD and the QR adaptive-coefficient FDFD were 2374 and 2317 s, respectively, when the FDFD sparse linear system was iteratively solved by the flexible generalized minimal residual method with preconditioning of the adaptive complex frequency and geometric multigrid (Xu et al., 2021a) on the 30 supercomputer nodes. Therefore, for this salt-dome model, the QR adaptive-coefficient FDFD proposed in this paper can reduce the computational time required by the existing CG adaptive-coefficient FDFD.

Figure 9. Slice of the three-dimensional SEG/EAGE salt-dome model.
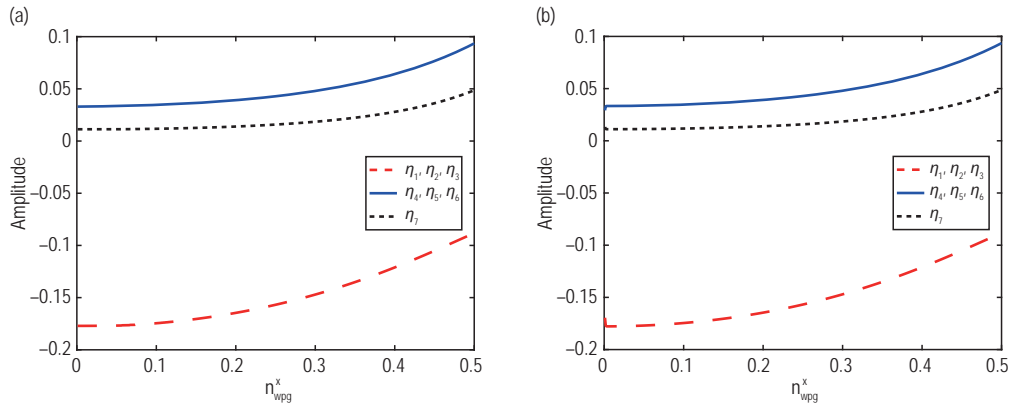
Figure 10. (a) Conjugate gradient adaptive finite-difference frequency domain (FDFD) coefficients (Xu et al., 2021b) and (b) QR adaptive FDFD coefficients corresponding to the three-dimensional SEG/EAGE salt-dome model ($r_1 = 1$ and $r_2 = 1$).
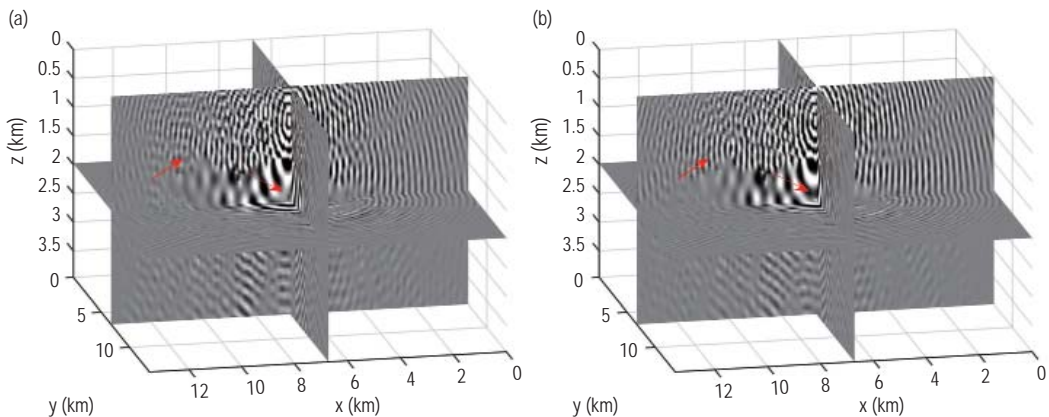
13
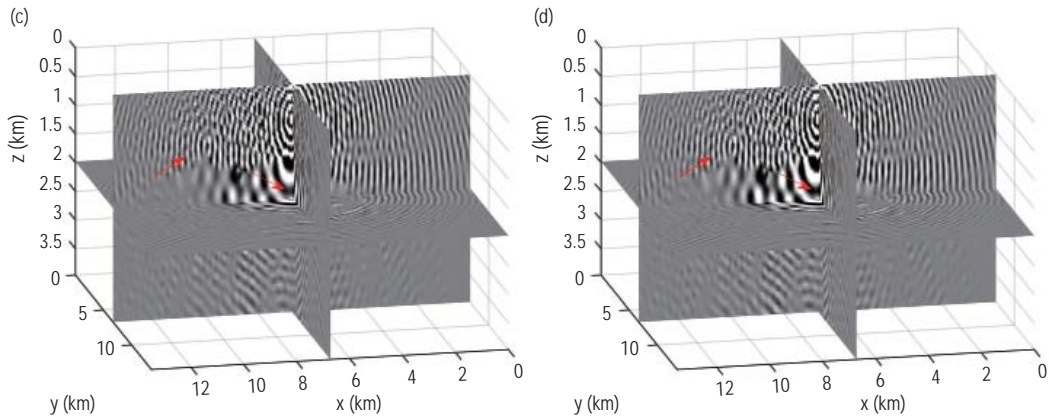
Figure 11. Monochromatic slices obtained by different methods for the three-dimensional SEG/EAGE salt-dome model at 10 Hz. (a) ADM optimal 27-point finite-difference frequency domain (FDFD) method, (b) conjugate gradient adaptive-coefficient 27-point FDFD method, (c) QR adaptive-coefficient 27-point FDFD method, and (d) reference solution (high-order FDFD method with 72nd order in the x-, y-, and z-directions). The red arrows indicate the regions where the differences are more obvious.
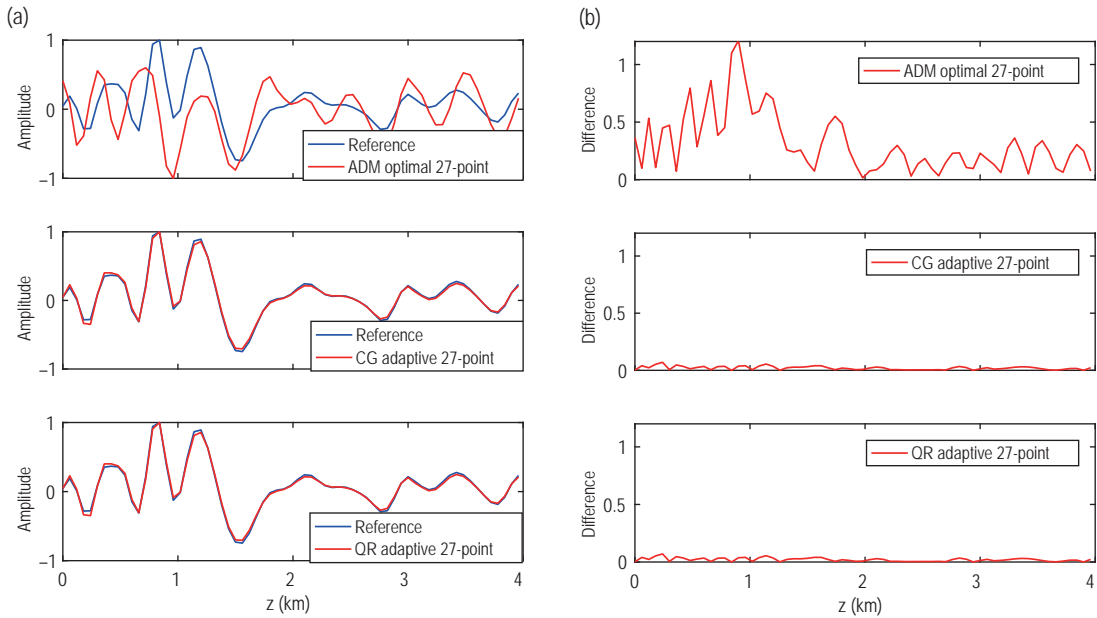
Figure 12. Comparison of the vertical single traces of the single-frequency slices (x = 13500 m and y = 13500 m) of the salt-dome model at 10 Hz between the reference solution (high-order finite-difference frequency domain (FDFD) method with 72nd order in the x-, y-, and z-directions) and the results obtained by the ADM optimal 27-point FDFD, conjugate gradient adaptive-coefficient 27-point FDFD, and QR adaptive-coefficient 27-point FDFD methods for the three-dimensional SEG/EAGE salt-dome model. Comparison of (a) amplitudes and (b) amplitude differences.
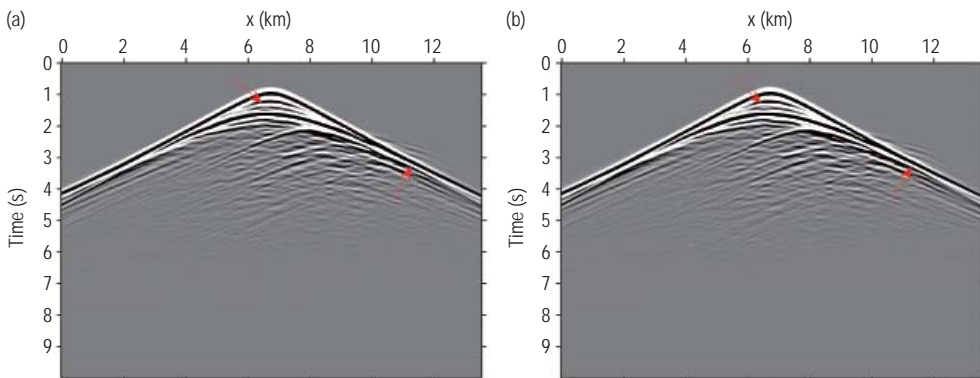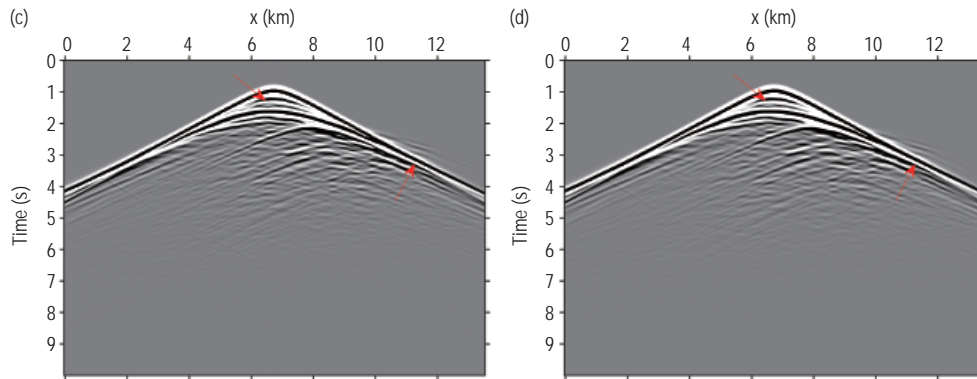
Figure 13. Time-domain seismograms obtained by different methods for the three-dimensional SEG/EAGE salt-dome model. (a) ADM optimal 27-point finite-difference frequency domain (FDFD) method, (b) conjugate gradient adaptive-coefficient 27-point FDFD method, (c) QR adaptive-coefficient 27-point FDFD method, and (d) reference solution (high-order FDFD method with 72nd order in the *x*-, *y*-, and *z*-directions). The red arrows indicate the regions where the differences are more obvious.

Conclusions

Herein, a novel method for calculating adaptive FDFD coefficients based on QR decomposition is proposed. The method can avoid the requirement of numerical integration, CG optimization, sequential initial value selection, and smooth regularization involved in the existing methods for calculating adaptive FDFD coefficients. The comparison of computational times required for generating the adaptive-coefficient lookup tables reveals that the proposed QR method can significantly improve the efficiency of calculating adaptive FDFD coefficients compared with the CG methods based on numerical integration, CG optimization, and sequential initial value selection. The numerical wavefield simulation results of the 3D homogeneous model, layered model, and SEG/EAGE salt-dome model show that the adaptive-coefficient FDFD method based on QR decomposition can achieve accuracy identical to that of the adaptive-coefficient FDFD method based on CG optimization while requiring less computational time. The key concept underlying the proposed method is the use of QR decomposition to solve the discrete linear least-squares problem obtained by substituting plane-wave solutions into the FDFD scheme. This method can be generalized to determine the adaptive FDFD coefficients of viscoacoustic and elastic wave equations. Since the proposed QR method of calculating adaptive FDFD coefficients is easy to implement and has high computational efficiency, it is anticipated to promote further practical applications of adaptive-coefficient FDFD methods in seismic wavefield simulations.

Acknowledgements

References

Aghamiry, H. S., Gholami, A., Combe, L., and Operto, S. 2022, Accurate 3D frequency-domain seismic wave modeling with the wavelength-adaptive 27-point finite-difference stencil: A tool for full-waveform inversion: Geophysics, **87**(3), R305–R324.

Chen, J. B., 2012, An average-derivative optimal scheme for frequency-domain scalar wave equation: Geophysics, **77**(6), T201–T210.

Chen, J. B., 2014, A 27-point scheme for a 3D frequency-domain scalar wave equation based on an average-derivative method: Geophysical Prospecting, **62**(2), 258–277.

Dablain, M. A., 1986, The application of high-order differencing to the scalar wave equation: Geophysics, **51**(1), 54–66.

Fan, N., Zhao, L. F., Xie, X. B., Tang, X. G., and Yao, Z. X., 2017, A general optimal method for a 2D frequency-domain finite-difference solution of scalar wave equation: Geophysics, **82**(3), T121–T132.

Gao, J., Xu, W., Wu, B., Li, B., and Zhao, H., 2018, Trapezoid grid finite difference seismic wavefield simulation with uniform depth sampling interval: Chinese Journal of Geophysics, **61**(8), 3285–3296.

Golub, G. H., and Van Loan, C. F., 2013, Matrix computations: Johns Hopkins University Press, Baltimore, US, 233–302.

Harris, C. R., Millman, K. J., Van Der Walt, S. J., et al., 2020, Array programming with NumPy: Nature, **585**(7825), 357–362.

Jo, C. H., Shin, C., and Suh, J. H., 1996, An optimal 9-point, finite-difference, frequency-space, 2-D scalar wave extrapolator: Geophysics, **61**(2), 529–537.

Komatitsch, D., and Martin, R., 2007, An unsplit convolutional perfectly matched layer improved at grazing incidence for the seismic wave equation: Geophysics, **72**(5), SM155–SM167.

Liu, Q. H., and Tao, J., 1997, The perfectly matched layer for acoustic waves in absorptive media: The Journal of the Acoustical Society of America, **102**(4), 2072–2082.

Min, D. J., Shin, C., Kwon, B. D., and Chung, S., 2000, Improved frequency-domain elastic wave modeling using weighted-averaging difference operators: Geophysics, **65**(3), 884–895.

Operto, S., Amestoy, P., Aghamiry, H., et al., 2023, Is 3D frequency-domain FWI of full-azimuth/long-offset OBN data feasible? The Gorgon data FWI case study: The Leading Edge, **42**(3), 173–183.

Petra, C. G., Schenk, O., and Anitescu, M., 2014, Real-time stochastic optimization of complex energy systems on high-performance computers: Computing in Science and Engineering, **16**(5), 32–42.

Petra, C. G., Schenk, O., Lubin, M., and Gärtner, K., 2014, An augmented incomplete factorization approach for computing the Schur complement in stochastic optimization: SIAM Journal on Scientific Computing, **36**(2), C139–C162.

Pratt, R. G., 1990, Frequency-domain elastic wave modeling by finite differences: A tool for crosshole seismic imaging: Geophysics, **55**(5), 626–632.

Pratt, R. G., and Worthington, M. H., 1990, Inverse theory applied to multi-source cross-hole tomography, Part I: acoustic wave-equation method: Geophysical Prospecting, **38**(3), 287–310.

Ren, Z., and Liu, Y., 2013, A hybrid absorbing boundary condition for frequency-domain finite-difference modelling: Journal of Geophysics and Engineering, **10**(5), 054003, doi: 10.1088/1742-2132/10/5/054003.

Rupp, K., Tillet, P., Rudolf, F., et al., 2016, ViennaCL--linear algebra library for multi-and many-core architectures: SIAM Journal on Scientific Computing, **38**(5), S412–S439.

Shin, C., and Sohn, H., 1998, A frequency-space 2-D scalar wave extrapolator using extended 25-point finite-difference operator: Geophysics, **63**(1), 289–296.

Štekl, I., and Pratt, R. G., 1998, Accurate viscoelastic modeling by frequency-domain finite differences using rotated operators: Geophysics, **63**(5), 1779–1794.

Tournier, P. H., Jolivet, P., Dolean, V., Aghamiry, H. S.,

Operto, S., and Riffo, S., 2022, 3D finite-difference and finite-element frequency-domain wave simulation with multilevel optimized additive Schwarz domain-decomposition preconditioner: A tool for full-waveform inversion of sparse node data sets: Geophysics, **87**(5), T381–T402.

Virieux, J., 1986, P-SV wave propagation in heterogeneous media: Velocity-stress finite-difference method: Geophysics, **51**(4), 889–901.

Wang, E., Ba, J., and Liu, Y., 2018, Time-space-domain implicit finite-difference methods for modeling acoustic wave equations: Geophysics, **83**(4), T175–T193.

Xu, J., Hu, H., Zhan, Q., Zhong, Y., and Liu, Q. H., 2023, Nearly perfectly matched layer implementation for time domain spectral element modelling of wave propagation in 3D heterogeneous and anisotropic porous media: Journal of Applied Geophysics, **208**, 104870, doi: 10.1016/j.jappgeo.2022.104870.

Xu, W., and Gao, J., 2018, Adaptive 9-point frequency-domain finite difference scheme for wavefield modeling of 2D acoustic wave equation: Journal of Geophysics and Engineering, **15**(4), 1432–1445.

Xu, W., Zhong, Y., Wu, B., Gao, J., and Liu, Q. H., 2021a, Adaptive complex frequency with V-cycle GMRES for preconditioning 3D Helmholtz equation: Geophysics, **86**(5), T349–T359.

Xu, W., Wu, B., Zhong, Y., Gao, J., and Liu, Q. H., 2021b, Adaptive 27-point finite-difference frequency-domain method for wave simulation of 3D acoustic wave equation: Geophysics, **86**(6), T439–T449.

Zhang, H., Liu, H., Lui, L., Jin, W., and Shi, X., 2014, Frequency domain acoustic equation high-order modeling based on an average-derivative method: Chinese Journal of Geophysics, **57**(5), 1599–1611.

Zhang, J. H., and Yao, Z. X., 2013, Optimized finite-difference operator for broadband seismic wave modeling: Geophysics, **78**(1), A13–A18.

Zhang, Y., Gao, J., and Peng, J., 2018, Variable-order finite difference scheme for numerical simulation in 3-D poroelastic media: IEEE Transactions on Geoscience and Remote Sensing, **56**(5), 2991–3001.

Xu Wen-Hao received his Ph.D. degree in Information and Communication Engineering from Xi'an Jiaotong University in 2022 and has been working as an assistant researcher in the School of Earth Science and Engineering, Hohai University, since 2022. His main research interests are seismic wavefield simulation and seismic parameter inversion.